# A geometric factor calculation method based on the isotropic flux assumption*

ZHAO Xiao-Yun(赵小芸)[1;1)] WANG Huan-Yu(王焕玉)[1;2)] WU Feng(吴峰)[2] MENG Xiang-Cheng(孟祥承)[1]
MA Yu-Qian(马宇蒨)[1] LU Hong(卢红)[1] WANG Hui(王辉)[1] WANG Ping(王平)[1]
LI Xin-Qiao(李新乔)[1] XU Yan-Bin(徐岩冰)[1] SHI Feng(石峰)[1] JIANG Wen-Qi(蒋文奇)[1]
AN Zhen-Hua(安正华)[1] YU Xiao-Xia(于晓霞)[1] LIU Han-Yi(刘汉一)[1]

[1] Institute of High Energy Physics, Chinese Academy of Sciences, Beijing 100049, China
[2] Department of Modern Physics, University of Science and Technology of China, Hefei 230026, China

**Abstract:** One of the instruments onboard the China Seismic Electromagnetic Satellite (CSES) is the Low Energy Particle Detector (LEPD). The primary objective of LEPD is to provide measurements of the fluxes, energy spectra and pitch angles of 100 keV to 10 MeV electrons and protons from 2 to 50 MeV in the Earth's magnetosphere. The geometric factor is one of the principle parameters of a detector, which converts the physical quantity–count rate to the particle quantity-flux. In this paper, we calculated the geometric factor of LEPD via computer modeling of an isotropic radiation environment. It was first demonstrated that the radiation intensity related should obey a cosine-law, then a general sampling method of generating this distribution via GPS of GEANT4 was explained. Furthermore, combined with flux normalization, a comparison of the geometric factor calculation of a set of 2-layer detectors with different shapes (cylinder, truncated cone and rectangle) was performed. Results show a generally good agreement between simulation and analytical calculations for the cylinder and truncated cone detectors, and the result of the rectangular one, for which there is no accurate analytical formula, is consistent with the previous simulated results by others. As a practical instance of the 2-layer rectangle detector, the geometric factor of LEPD is 10.336±0.036 $cm^2$·sr for 10 MeV proton and 8.211±0.032 $cm^2$·sr for 8 MeV electron.

**Key words:** LEPD, geometric factor, isotropy, GEANT4, cosine distribution, flux normalization

**PACS:** 93.90.+y, 02.70.Uu **DOI:** 10.1088/1674-1137/37/12/126201

## 1 Introduction

The possible interrelation between high-energy particle fluxes (energy about several tens of MeV) and the seismicity of Earth was first observed in MARIA experiment onboard Salyut-7 orbital station in 1985 [1]. Later on, more satellite-borne experiments were carried out to study how seismic activity influences terrestrial surroundings and the ionosphere and magnetosphere in particular. Such experiments include: ELECTRON onboard INTERCOSMOS-BULGARIA-1300 and METEOR-3 [2, 3], MARIA-2 onboard MIR [4], GAMMA-1 onboard GAMMA [5], and PET of SAMPEX [6], etc. Results of these experiments confirmed the correlation between short-term sharp increases of particle intensities and seismic processes, moreover the temporal and spacial correlation between the earthquakes and the fluctuations of particle intensity was found [7]. As a result, more effort was devoted into this area to study the possibility of developing this phenomena as an earthquake prediction method. A new advance in this field is related to the proposed China Seismic Electromagnetic Satellite (CSES), the goals for which are to systematically study the electromagnetic waves linked to earthquakes, and to evaluate prognostic capabilities of the cosmic precursors of earthquakes. The scientific payload of the CSES is therefore composed of several types of sensors measuring electric field, magnetic field, plasma and particles. One of the instruments onboard the CSES is the Low Energy Particle Detector(LEPD), which is intended for the measurement of the fluxes of energetic electrons in the energy range: 100 keV–10 MeV, and protons in the energy range: 2–50 MeV. The polar orbit of the satellite (500 km altitude, heliosynchronous) and

Received 19 February 2013, Revised 2 April 2013
* Supported by CSES project
1) E-mail: xyzhao@ihep.ac.cn
2) E-mail: wanghy@ihep.ac.cn

its lifetime of 5 years will allow the survey of all the seismically active regions of the globe.

The LEPD instrument is designed to have a large geometric factor and a high energy resolution. The instrument (see Fig. 1) has a ±37° field of view. The beam path elements include a 40 μm aluminum window, two double-sided silicon strip detector (DSSD), and a CsI(Tl) scintillator. The two DSSD detectors are solid-state silicon detectors, which are square (50 mm×50 mm) in shape with thickness of 142 μm and 300 μm, respectively. The CsI(Tl) crystal is the calorimeter of this detector, dimension of which is 70 mm×70 mm×12 mm(T). The DSSDs and the CsI(Tl) together compose the $\Delta E$-$E$ telescope [8], a typical method for electron and proton identification in this energy range, and these three detectors are surrounded by a set of plastic scintillators that are used to veto uninterested entries. The detailed introduction of the electronics for LEPD and the experimental measurements of DSSDs were introduced by Wu et al [9].

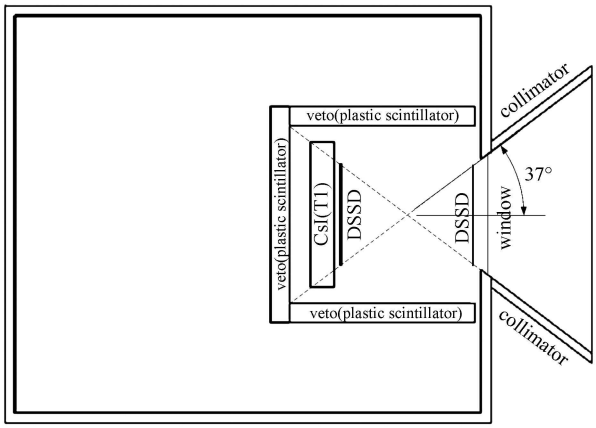


Fig. 1. Structure of LEPD.

Geometric factor calculations have an important application in the data analysis of a wide variety of experiments involving space-borne detectors. In this paper, we introduced a method of geometric factor calculation on assumption that the space-borne detector is located in an isotropic environment, which refers to uniformity of particle flux in all directions. In order to construct such an environment, we first demonstrated what kind of angular distribution the radiation intensity should have. Then a method based on it was applied in the calculation of the geometric factor of a 2-layer detector. The meaning of this method is the truncated cone and circular cylinder type detectors have rather accurate analytic formula [10], whereas the rectangle detector only has an approximate and complicated formula [11] that is applicable for limited situations.

## 2 Method

Isotropic radiation has the same intensity regardless of the direction of measurement [12]. As a result, any point inside the incident surface should get a constant value of intensity

$$\frac{\mathrm{d}N}{\mathrm{d}\Omega \mathrm{d}A_{\mathrm{eff}}}=\text{Constant}, \tag{1}$$

where $\mathrm{d}N$ stands for particles emitted in a solid angle $\mathrm{d}\Omega$ and from an effective area $\mathrm{d}A_{\mathrm{eff}}$. On the basis of Eq. (1), demonstration of the radiation intensity's distribution is given as follows.

### 2.1 The cosine-law

Meaning of the parameters that appeared in Fig. 2 are listed as below

1) $\mathrm{d}A$: an arbitrary surface element on the incident surface;

2) $\mathrm{d}A_0$: an arbitrary surface element on the detector;

3) $\theta$: the angle between the surface normal of $\mathrm{d}A$ and the direction of $\mathrm{d}A_0$;

4) $\alpha$: the angle between the surface normal of $\mathrm{d}A_0$ and the direction of $\mathrm{d}A$;

5) $\mathrm{d}A_\perp$: the projected area of $\mathrm{d}A$ seen looking along $\mathrm{d}A_0$;

6) $\mathrm{d}A_{0\perp}$: the projected area of $\mathrm{d}A_0$ seen looking along $\mathrm{d}A$;

7) $r$: distance from $\mathrm{d}A$ to $\mathrm{d}A_0$;

8) $I(\theta, \phi)$: radiation intensity ((particles)$\mathrm{s}^{-1}\cdot\mathrm{cm}^{-2}\cdot\mathrm{sr}^{-1}$) is defined as a function of polar angle $\theta$ and azimuthal angle $\phi$ in the spherical coordinates of the source surface element $\mathrm{d}A$;

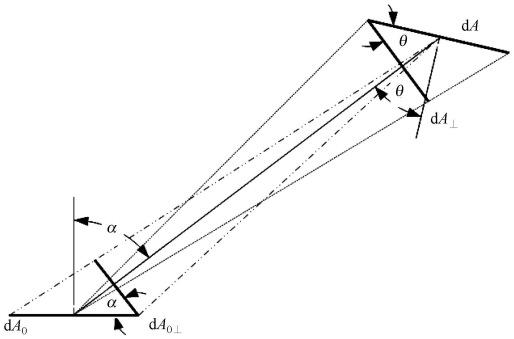


Fig. 2. Solid angles of $\mathrm{d}A_0$ and $\mathrm{d}A$ subtended to each other.

If we take $\mathrm{d}A_0$ as a research object, then $\mathrm{d}A$ can be treated as a point, so the solid angle of $\mathrm{d}A_0$ subtended to $\mathrm{d}A$ is given as

$$\mathrm{d}\Omega_0=\frac{\mathrm{d}A_0\cos\alpha}{r^2}. \tag{2}$$

Correspondingly, the solid angle of $\mathrm{d}A$ subtended to $\mathrm{d}A_0$ is given by

$$\mathrm{d}\Omega=\frac{\mathrm{d}A\cos\theta}{r^2}. \tag{3}$$

Thus numbers of emitted particles in the solid angle $\mathrm{d}\Omega_0$ should be

$$\mathrm{d}N=I(\theta,\phi)\mathrm{d}\Omega_0\mathrm{d}A. \tag{4}$$

Assuming $I_0$ is the radiation intensity, which means the constant term of Eq. (1)

$$\frac{\mathrm{d}N}{\mathrm{d}\Omega\mathrm{d}A_{\mathrm{eff}}}=\frac{I(\theta,\phi)\mathrm{d}\Omega_0\mathrm{d}A}{\mathrm{d}\Omega\mathrm{d}A_{0\perp}}=I_0. \tag{5}$$

We obtain

$$I(\theta,\phi)=I_0\cos\theta. \tag{6}$$

As a result, the radiation intensity has a cosine distribution. The cosine-law refers to the fact that the radiation intensity from a surface area in a particular direction is proportional to the cosine of the angle between that direction and the surface normal. This is also illustrated in Fig. 3. Each wedge in the diagram represents an equal angle $\mathrm{d}\Omega$, and the emission rate is proportional to the area of the wedge. So the maximum rate appears when $\theta=0°$, and diminishes while $\theta$ increases and finally is zero when $\theta=90°$.

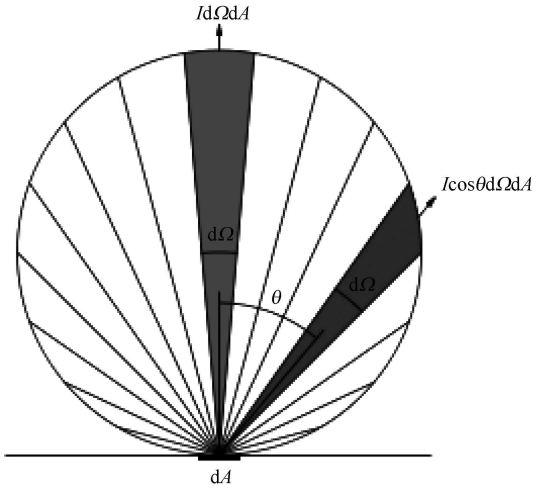


Fig. 3. Radiation intensity ($\mathrm{s}^{-1}\cdot\ \mathrm{cm}^{-2}\cdot\ \mathrm{sr}^{-1}$) in a normal and off-normal direction for cosine-law.

## 2.2 The probability density function

Under the known condition of the cosine distribution for radiation intensity, the probability density distributions for polar angle and azimuthal angle can be deduced.

Suppose the number of emitted particles from the source surface element $\mathrm{d}A$ is $N_0$, then it can be calculated by integrating the cosine law

$$N_0=\int_0^{2\pi}\mathrm{d}\phi\int_0^{\frac{\pi}{2}}I_0\cos\theta\sin\theta\mathrm{d}\theta. \tag{7}$$

Therefore $I_0=N_0/\pi$, since emitted particles in solid angle $\mathrm{d}\omega$ is

$$\mathrm{d}n=I(\theta,\phi)\mathrm{d}\omega=\frac{N_0}{\pi}\cos\theta\sin\theta\mathrm{d}\theta\mathrm{d}\phi. \tag{8}$$

If we label $\mathrm{d}n_\phi$ as the number of emitted particles in the region of any allowed $\theta$ value and in the azimuthal angular range $\phi$–$\phi$+$\mathrm{d}\phi$, and mark $\mathrm{d}n_\theta$ as the counterpart of any allowed $\phi$ value and in the polar angular range $\theta$–$\theta$+$\mathrm{d}\theta$, then the probability density function is given by

$$\begin{aligned} f(\phi) &= \frac{1}{N_0}\frac{\mathrm{d}n_\phi}{\mathrm{d}\phi},\\ f(\theta) &= \frac{1}{N_0}\frac{\mathrm{d}n_\theta}{\mathrm{d}\theta}, \end{aligned} \tag{9}$$

where

$$\begin{aligned} \mathrm{d}n_\phi &= \frac{N_0}{\pi}\mathrm{d}\phi\int_0^{\frac{\pi}{2}}\cos\theta\sin\theta\mathrm{d}\theta,\\ \mathrm{d}n_\theta &= \frac{N_0}{\pi}\cos\theta\sin\theta\mathrm{d}\theta\int_0^{2\pi}\mathrm{d}\phi, \end{aligned} \tag{10}$$

thus

$$\begin{aligned} f(\phi) &= \frac{1}{2\pi},\ \phi\in[0,2\pi],\\ f(\theta) &= \sin(2\theta),\ \theta\in\left[0,\frac{\pi}{2}\right]. \end{aligned} \tag{11}$$

The probability distribution of $\theta$ is shown in Fig. 4.

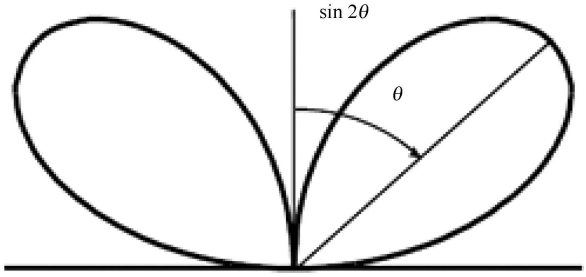


Fig. 4. Probability distribution of polar angle $\theta$ [13].

## 2.3 Implementation

To ensure the source density is homogeneous everywhere, the incident position should have a uniform distribution. In GEANT4 [14] simulation, with the probability density function, one can achieve the desired distribution by sampling or by invoking build-in functions via GPS (General Particle Source) [15], nevertheless they are identical in nature.

In this section, the above distribution is implemented generally by using GPS, which is part of the GEANT4 toolkit for Monte-Carlo, high-energy particle transport.

Specifically, it allows the specifications of the spectral, spatial and angular distribution of the primary source particles.

A sphere which encircles the detector completely was set as the incident surface to simplify the mathematics.

1) Position sampling

(1) Random numbers

In a spherical coordinate system, the probability density function of random variables $\theta$ and $\phi$ obey uniform distribution

$$f(\theta) = \frac{1}{2}\sin\theta,\ \theta\in[0,\ \pi], \tag{12}$$

$$h(\phi) = 1,\ \phi\in[0,\ 2\pi]. \tag{13}$$

Then, according to the method of inverse function of continuous random variable, in the interval $[a,\ b]$, continuous random variable $x$ should be sampled as Eq. (14) to obey its probability density function $f(x)$.

$$\xi=\frac{\int_0^x f(t)\mathrm{d}t}{\int_a^b f(t)\mathrm{d}t}, \tag{14}$$

where $\xi$ is a uniform random number in the interval [0, 1]. Thus

$$\theta=\arccos(1-2\xi),\quad \phi=2\pi\xi. \tag{15}$$

(2) Position coordinates

With the specified radius of sphere $R$, $\theta$ and $\phi$ sampled in step (1), the position coordinates $(x,\ y,\ z)$ are given by

$$\begin{aligned} x &= R\times\sin\theta\times\cos\phi,\\ y &= R\times\sin\theta\times\sin\phi,\\ z &= R\times\cos\theta. \end{aligned} \tag{16}$$

(3) New coordinates base vector

A new coordinate base vector is needed, which can be used to perform the coordinate transformation for the direction vector from the detector system into the local incident sphere coordinate system. The new axes are defined as follows:

$Z$ axis is the vector of $(x,\ y,\ z)$; $X$ axis is achieved by vector product of the new $Z$ vector and the $Z$ vector of the detector system; $Y$ axis is the vector product of the new $X$ vector and the new $Z$ vector. After unitization, the new coordinate base vectors are given as $(S_1,\ S_2,\ S_3)$.

2) Angular sampling

(1) Random numbers

As demonstration shows, the probability density function of the polar angle is determined by Eq. (11),

$$\xi = \frac{\int_0^\theta \sin(2t)\mathrm{d}t}{\int_0^{\pi/2} \sin(2t)\mathrm{d}t}, \tag{17}$$

$$\xi = \int_0^\phi \frac{1}{2\pi}\mathrm{d}y, \tag{18}$$

thus we have

$$\sin\theta=\sqrt{\xi},\ \cos\theta=\sqrt{1-\xi},\ \phi=2\pi\xi. \tag{19}$$

(2) Direction Vector $P$

The three components of direction vector $P$ are given by

$$\begin{aligned} p_x&=-\sin\theta\times\cos\phi,\\ p_y&=-\sin\theta\times\sin\phi,\\ p_z&=-\cos\theta. \end{aligned}$$

(3) Final incident direction vector $F$

In this step, the new axis vector $(S_1,\ S_2,\ S_3)$ mentioned in step 3) of position sampling is used.

$$A=\begin{pmatrix} S_1.x & S_2.x & S_3.x\\ S_1.y & S_2.y & S_3.y\\ S_1.z & S_2.z & S_3.z \end{pmatrix}. \tag{20}$$

The matrix composed by coordinate base vectors is an orthogonal matrix,

$$A\times A^{\mathrm{T}}=I. \tag{21}$$

When an orthogonal matrix multiplies a vector, the modulus of the vector doesn't change, but its direction does.

Consequently, the effect of multiplication between the new coordinate base vectors $(S_1,\ S_2,\ S_3)$ and the direction vector is just a rotation of the latter by a certain angle, and this gives the final incident direction vector $(f_x,\ f_y,\ f_z)$.

$$\begin{aligned} \begin{pmatrix} f_x\\ f_y\\ f_z \end{pmatrix} &= \begin{pmatrix} S_1.x & S_2.x & S_3.x\\ S_1.y & S_2.y & S_3.y\\ S_1.z & S_2.z & S_3.z \end{pmatrix}\begin{pmatrix} p_x\\ p_y\\ p_z \end{pmatrix}\\ &= \begin{pmatrix} p_x\times S_1.x+p_yS_2.x+p_zS_3.x\\ p_x\times S_1.y+p_yS_2.y+p_zS_3.y\\ p_x\times S_1.z+p_yS_2.z+p_zS_3.z \end{pmatrix}. \end{aligned} \tag{22}$$

3) The resultant position and angle distribution

In Fig. 5, from left to right they are the position distribution projected on $XY$, $ZX$, $ZY$ plane, the angular distribution of $\theta$ versus $\phi$, and $\cos\theta$ versus $\phi$.

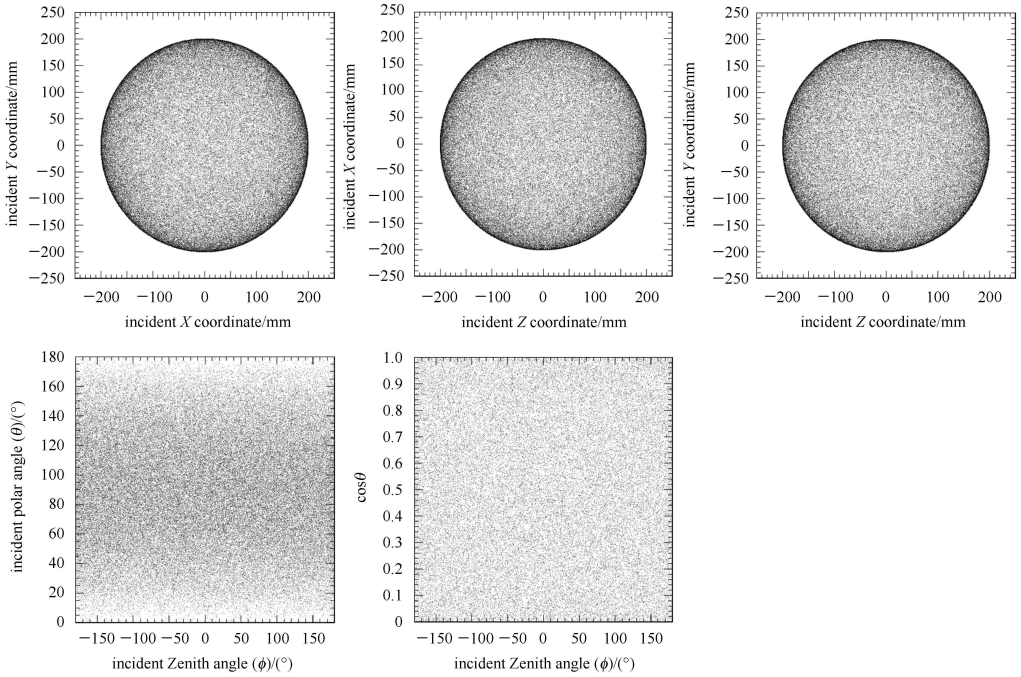


Fig. 5. The distribution of position and angle been sampled for isotopic radiation (from left to right they are the position distribution of incident $X$ coordinate versus $Y$ coordinate, incident $Z$ coordinate versus $X$ coordinate, incident $Z$ coordinate versus $Y$ coordinate, and the angular distribution of $\theta$ versus $\phi$, and cos$\theta$ versus $\phi$).

It is seen from Fig. 5 that the position distribution is uniform on the sphere, and $\phi$ is uniform in [0, 2$\pi$], while $\theta$ is not uniform in [0, $\pi$], but cos($\theta$) is uniform in [0, 1] which is just in accord with the definition of isotropy.

## 3 Application

Geometric factor ($G$) [10] is defined as the counts ($N_{\rm d}$) received by a detector per unit time interval divided by the spatial differential flux $j$ (cm$^{-2}\cdot$ s$^{-1}\cdot$ sr$^{-1}$).

$$G=\frac{N_{\rm d}}{j}. \tag{23}$$

Before simulation commences, flux normalization should be done to make one-to-one correspondence relationship between the number of incident particles and the flux.

### 3.1 Normalization

On condition of isotropic radiation environment and a spherical incident surface, the number of particles $N_r$ traversing the sphere is determined by an integral of the differential flux $j$ over the source area and the solid angle [16].

$$N_r=\iint j{\rm d}s{\rm d}\Omega=\pi\int j{\rm d}s=4\pi^2R^2j. \tag{24}$$

By counting the received Field of View (FOV) incidents on the detector $N_{\rm d}$, we obtained the ideal geometric factor by Eq. (23). The so-called FOV incidents are chosen on condition that the spatial line determined by the position coordinates and direction vector of the incident point intersects with both layers of the detector.

Table 1 lists the results of comparison for 4 different simple detectors (shown in Fig. 6). Within the error range, it agrees well with the formula and other method.

Table 1. Comparison of the geometric factors calculation for 4 different detectors.

| type | $G_{\rm ana}$/(cm$^2\cdot$sr) | $G_{\rm sim}$/(cm$^2\cdot$sr) |
|---|---|---|
| A | 9.870 | 9.769±0.111 |
| B | 0.709 | 0.764±0.031 |
| C | 5.289 | 5.262±0.081 |
| D | 0.482 | 0.518±0.026 |

$G_{\rm ana}$=geometric factor calculated analytically
$G_{\rm sim}$ [2)]=geometric factor given by simulation

A. 1-layer circle detector with radius $R$=1 cm;

B. 2-layer circular cylinder detector with radius $R$= 1 cm, and $\theta$=30°;

C. 2-layer truncated cone detector with radius $R_1$= 1 cm, $R_2$=2 cm, and $\theta$=30°;

D. 2-layer rectangular detector with side length $a$= 2 cm, $b$=1 cm, and $\theta$=30°.

A practical instance of the 2-layer rectangular detector is a space dark matter detector with dimension of

1) Eq. (24) is applicable under the isotropic flux assumption
2) flux=$10^4$ cm$^{-2}\cdot$ s$^{-1}$

$a$=150 cm, $b$=60 cm and the distance between the layers is 72 cm. The result of the geometric factor of this detector presented in the thesis [17] coincides with our result, which is 0.60 $m^2$·sr and 0.621±0.028 $m^2$·sr respectively.

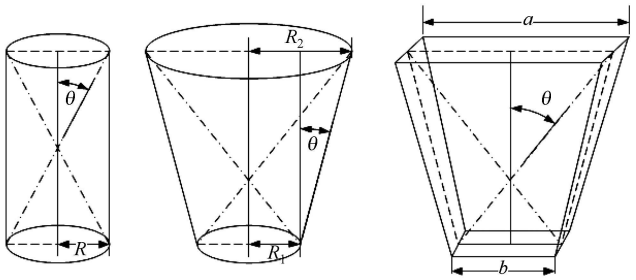


Fig. 6. Schematic diagram of the type B, C, D detectors.

### 3.2 Geometric factor for LEPD

By using the above simulation method we calculated the geometric factor of LEPD (Fig. 7).

The solid line stands for the ideal geometric factor of this detector, the dashed-dotted line and the dashed line respectively represent the actual geometric factor of electron and proton varies with its kinetic energy. As a result, the difference between the dashed-dotted line (or dashed line) and the black solid line is mainly caused by the detection efficiency of LEPD, which can be explained by the following:

Because protons and electrons out of the interested energy range can penetrate the 12 mm-thick CsI(Tl) and hit the surrounding plastic scintillators (PS), entries with deposited energy in the PS larger than a typical threshold (e.g.∼100 keV) would be vetoed. Therefore, the geometric factors for protons with energy more than 50 MeV and electrons more than 10 MeV declines. However, the major reason for the small value of geometric factor in the lower energy range is different for electrons and protons: the former are caused by multiple-scattering and the latter are due to a weaker penetrating power. Both these effects lead to a poor detection efficiency.

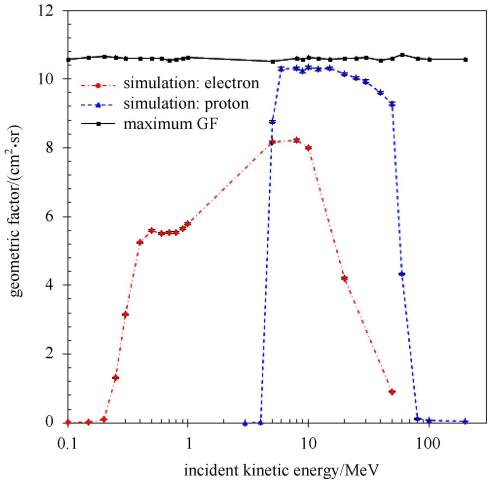


Fig. 7. Geometric Factor of LEPD.

## 4 Summary

In this paper, we demonstrated that it is the cosine distribution that radiation intensity should have to construct a global isotropic radiation environment around the detector in simulation, and deduced the probability density function correspondingly. This method was applied in the geometric factor calculation of a set of 2-layer detectors and of LEPD. Results of the former showed that simulation agrees with formula, and the simulation method is independent of layer shape; it is rather suitable for the 2-layer rectangular detector, as there's no accurate analytical formula for this type. Results for the latter show that LEPD has a large geometric factor in the interested energy range, and the maximum value is 10.336±0.036 $cm^2$·sr for 10 MeV proton and 8.211±0.032 $cm^2$·sr for 8 MeV electron.

*The author would like to acknowledge useful discussions on this subject with Dr. Zhicheng Tang of Institute of High Energy Physics, Chinese Academy of Sciences.*

## References

1 Voronov S A, Galper A M, Koldashov S V et al. Proc. 20th ICRC, 1987, Moscow, **4**: 451
2 Galper A M et al. Cosmic Research, 1989, **27**(5): 789–792
3 Voronov S A et al. Cosmic Research, 1990, **28**(5): 789–791
4 Galper A M, Koldashov S V, Voronov S A. Advances in Space Research, 1995, **15**(11): 131–134
5 Akimov V V et al. Space Science Reviews, 1988, **49**: 111–124
6 Baker D N et al. IEEE Trans. Geosciencies and Remote Sensing, 1993, **31**: 531
7 Galper A M, Koldashov S V, Voronov S A. Adv. Space Res, 1995, **15**(11): 131–134
8 XU Yan-Bing, WANG Huan-Yu, MENG Xiang-Cheng et al. Chinese Physics C (HEP & NP), 2010, **34**: 1846–1851
9 WU Feng, WANG Huan-Yu et al. Chin. Phys. C (HEP & NP), 2013, **37**(2): 026004
10 YE Zong-Hai. Space Particle Radiation Detection Technology. Beijing: Science Press. 1986. 261–268 (in Chinese)
11 Sullivan J D. Nuclear Instruments and Methods, 1971, **95**(1): 5–11
12 Khatib T, Mohamed A, Sopian K. Renewable and Sustainable Energy Reviews, 2012, **16**(5): 2864–2869
13 Greenwood J. Vacuum, 2002, **67**(2): 217–222
14 Agostinelli S et al. Nuclear Instruments and Methods in Physics Research Section A-Accelerators Spectrometers Detectors and Associated Equipment, 2003, **506**(3): 250–303
15 http://reat.space.qinetiq.com/gps/new_gps_sum_files/gps_sum.htm
16 Giovanni Santin. Normalisation Modelling Sources, 2007. Paris
17 ZHANG Yun-Long. The Study of an EM Calorimeter for Searching Dark Matter in Space. University of Science and Technology of China, 2011. 49–52 (in Chinese)